ChemComm

COMMUNICATION

View Article Online
View Journal | View Issue

Cite this: *Chem. Commun.*, 2025, **61**, 19628

Received 1st September 2025,
Accepted 11th November 2025

DOI: 10.1039/d5cc05041c

rsc.li/chemcomm

Tuning the fate of the triplet by changing the degree of branching in phenothiazine–trithienyltriazine nanoaggregates

Pietro Mancini,[a] Chiara Montanari,[a] Penelope Venturi,[a] Kusum Yadav,[b] Tommaso Bianconi,[cd] Eleonora Calzoni, [a] Alessio Cesaretti, [a] Rajneesh Misra *[b] and Benedetta Carlotti *[a]

Nanoaggregates of phenothiazine–trithienyltriazine compounds with a different degree of branching (TRZ1–3) were investigated in a water dispersion with time-resolved spectroscopy. Room temperature phosphorescence was highlighted for TRZ1, reactive oxygen species production for TRZ2, and red thermally activated delayed fluorescence for TRZ3. These aggregation induced emission materials hold great potential for imaging-guided photodynamic therapy.

In recent years, there has been significant interest in developing organic thermally-activated delayed fluorescence (TADF) materials for highly efficient electroluminescence in third-generation organic light-emitting diode (OLED) devices.[1,2] Unlike conventional fluorescence, TADF allows harnessing both the singlet and triplet excitons for emission *via* reverse intersystem crossing (rISC) from T_1 to S_1, enabled in fluorophores with a small singlet-to-triplet energy gap (ΔE_{ST}).[3] Such peculiar energetic conditions have been generally achieved in organic push–pull dyes bearing electron donor (D) and electron acceptor (A) units connected by π-linkers where the photoinduced intramolecular charge transfer (ICT) triggers effective triplet production *via* spin orbit charge transfer (SOCT) induced ISC.[4–7] Strikingly, by virtue of the low-cost, favorable photophysical features and excellent biocompatibility (being metal-free molecular structures), purely organic TADF materials show fascinating appeal also in the field of biomedicine.[8] In fact, the long-lived emission of TADF fluorophores makes them optimal probes for time-resolved luminescence imaging (TRLI), with the potential to eliminate the background autofluorescence from biological tissues and improve bioimaging resolution.[9,10] Beyond this, TADF molecules could also be used as new metal-free photosensitizers for photodynamic therapy (PDT) through interaction of the photogenerated T_1 state with molecular oxygen, leading to the production of toxic reactive oxygen species (ROS).[11,12] It is noteworthy that donor–acceptor molecules generally exhibit large nonlinear optical features, such as two-photon absorption (TPA), particularly when arranged in multibranched molecular structures.[13,14] The possibility to trigger emission and ROS generation in push–pull TADF chromophores with the low energetic, highly focused and deeply penetrating infrared radiation makes them particularly suitable for biomedicine in general and for imaging-guided TP-induced PDT in particular.[15,16] The highly hydrophobic donor–acceptor dyes generally need to be encapsulated in water-dispersed organic or polymeric nanoparticles for their biological use.[10]

In a previous work of ours, we have reported the synthesis and photophysical characterization in solution and in the solid state of three push–pull phenothiazine (D) and trithienyltriazine (A) derivatives, where the D/A units are linked through triple bonds and arranged in dipolar (**TRZ1**), quadrupolar (**TRZ2**), and octupolar (**TRZ3**) molecular structures (Fig. 1A).[17] We found large triplet production and small ΔE_{ST} for these molecules and gained clear evidence for orange/red TADF in solid-state thin films, with important implications for optoelectronic applications. Here, we explore the potential of these new fluorophores, exhibiting TADF in the biological transparency window, for use in the biomedical field. In particular, in the present work, we investigate their photophysics as water-dispersed organic nanoaggregates with conventional steady state and advanced time-resolved spectroscopy, with nanosecond and femtosecond resolution, in absorption and in emission, to unveil the occurrence of aggregation-induced delayed emission.[18–22] Moreover, we study the emissive behavior of these organic nanoparticles in a cellular environment through fluorescence microscopy as well as their phototoxicity against melanoma and breast cancer cells through the MTT assay coupled with ROS fluorimetric assay.

Absorption and emission spectra of **TRZ1–3** were investigated in dimethylsulphoxide (DMSO)/water (W) mixtures with

[a] *Department of Chemistry, Biology and Biotechnology and CEMIN, University of Perugia, via Elce di sotto 8, 06123 Perugia, Italy. E-mail: benedetta.carlotti@unipg.it*
[b] *Department of Chemistry, Indian Institute of Technology, Indore 453552, India. E-mail: rajneeshmisra@iiti.ac.in*
[c] *Department of Chemistry, University of Wisconsin-Madison, University Ave 1101, 53706 Madison (WI), USA*
[d] *Department of Physics, Politecnico di Milano, Piazza Leonardo da Vinci 32, Milan 20133, Italy*

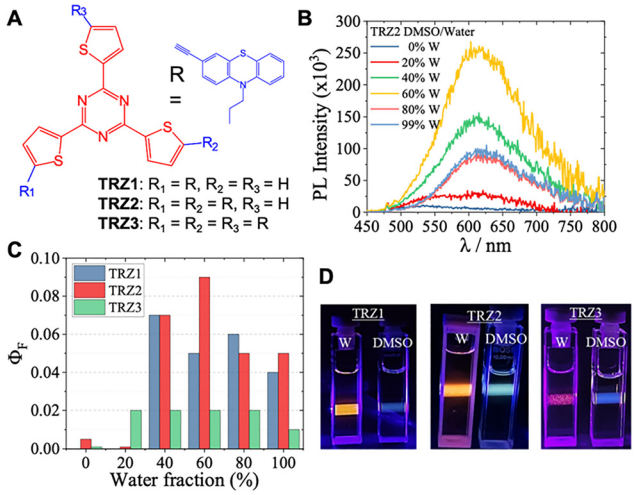

Fig. 1 (A) Molecular structures of the investigated compounds. (B) Emission spectra recorded for **TRZ2** in DMSO/water mixtures with different water amounts. (C) Fluorescence quantum yields measured for **TRZ1–3** in DMSO/water mixtures with different water fractions. (D) Pictures of the fluorescence triggered upon a blue laser excitation for **TRZ1–3** monomers (in DMSO) and aggregates (in water dispersion at 99%W).

different compositions (see Fig. 1B and Fig. S1, S2). DMSO is a good solvent for these molecules, whereas water is a poor solvent; upon exceeding 40% water content, aggregation of the organic dyes is triggered. Aggregate formation leads to small changes in the absorption spectra (Fig. S1) and to a strong enhancement in the fluorescence intensity (Fig. S2), proving a clear aggregation-induced emission (AIE) behavior.[20] A very low fluorescence was observed in pure DMSO.[17] On the other hand, a remarkable emission attributed to the aggregates was detected in DMSO/W mixtures above 40%W. The excitation spectra overlap well with the absorption spectra for the aggregates (Fig. S3–S5). The fluorescence quantum yields exhibit values of *ca.* 5% for the **TRZ1–2** and *ca.* 2% for the **TRZ3** aggregates in a water dispersion, significantly enhanced with the aggregation (Fig. 1C and Table S1). The fluorescence kinetics recorded by time correlated single photon counting (TC-SPC) in a 50 ns time window (Fig. S6) showed a multiexponential decay at large water amount in the mixture (Table S1), likely determined by the inhomogeneous nature of the formed aggregates.[20] Interestingly, the fluorescence emitted under a blue laser excitation looks negligible for the monomers in DMSO (only scattering from exciting light visible), while being bright orange (**TRZ1–2**) and red (**TRZ3**) for the aggregates in water dispersion (Fig. 1D). It is noteworthy that a large portion of the emission exhibited by these organic aggregates in water (Fig. S2) falls within the biological transparency window.

Femtosecond transient absorption measurements were carried out to uncover the photoinduced excited state dynamics for the **TRZ1–3** monomers in DMSO and aggregates in water dispersion (DMSO/W at 99%W). The time resolved absorption spectra recorded in the polar DMSO solvent (panel B of Fig. S12–S14) show a fast evolution from an excited-state absorption (ESA) characterized by two bands at *ca.* 570 and 670 nm (attributed to the locally excited singlet excited state, $S_{1,LE}$) to a single ESA peak at *ca.* 550 nm (assigned to the intramolecular charge transfer state, $S_{1,ICT}$). Global fitting of the data in DMSO revealed the presence of four exponential components (Fig. 2C): the first component with a lifetime of hundreds of fs assigned to $S_{1,LE}$, the second with a lifetime of *ca.* 2 ps assigned to diffusive solvation, the third with a lifetime of 27, 9.6 and 8.1 ps for **TRZ1–3** associated to the $S_{1,ICT}$, and a residual component not decaying in the investigated time window (Inf) associated with the population of T_1. The trend of decreasing $S_{1,ICT}$ lifetime with increasing the degree of branching may be due to the increased ICT character for the quadrupolar and octupolar relative to the dipolar derivatives.[23] When the ultrafast dynamics were investigated for the aggregates in water dispersion (Fig. 2A, B and Fig. S15–S17), a slower $S_{1,LE}$ to $S_{1,ICT}$ conversion was observed, with the $S_{1,LE}$ lifetime being *ca.* 2 ps under these experimental conditions. Similarly, the $S_{1,ICT}$ decay was found to occur in 290, 79, and 71 ps for the **TRZ1**, **TRZ2** and **TRZ3** aggregates, respectively. Such slower excited state deactivation may be determined by the restriction of intramolecular movements in the water-dispersed aggregates relative to the monomers.[19] An Inf component was revealed by the fitting of the femtosecond transient absorption results in water in all cases. The evolution-associated spectrum

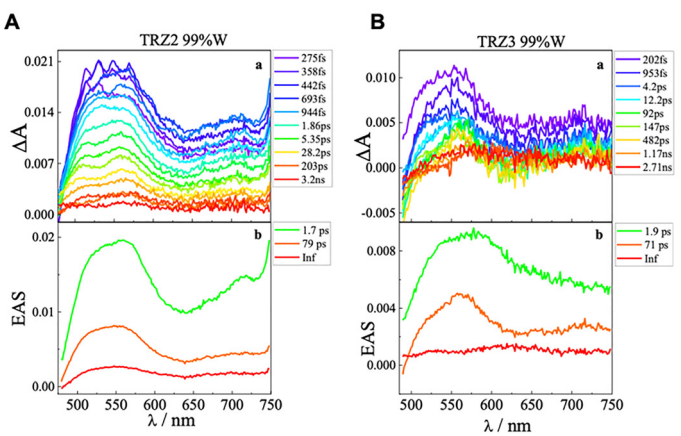

C

	τ_{TA} / ps			Assignment
	TRZ1	TRZ2	TRZ3	
DMSO	0.20	0.41	0.20	Solvation /$S_{1,LE}$
	2.6	2.6	2.4	Solvation
	27	9.6	8.1	$S_{1,ICT}$
	Inf	Inf	Inf	T_1
99%W	2.1	1.7	1.9	$S_{1,LE}$
	290	79	71	$S_{1,ICT}$
	Inf	Inf	Inf	$S_{1,ICT}$ /T_1

Fig. 2 Femtosecond transient absorption data obtained for **TRZ2** (A) and **TRZ3** (B) in water dispersion (99%W). (a) Transient absorption spectra at different delays after excitation. (b) Evolution associated spectra (EAS) and lifetimes obtained from the global analysis of the data. (C) Table summarizing the results of global analysis in terms of lifetimes and assignment of the components.

(EAS in Fig. 2A and B) for the Inf component was found to be more similar to the singlet excited state absorption for **TRZ1** and **TRZ2** (consistent with the nanosecond decay components observed for the aggregates vis TC-SPC) while being a triplet-like absorption spectrum for **TRZ3**. This finding suggests faster triplet production in **TRZ3** relative to the other compounds, likely due to its increased SOCT.

Nanosecond transient absorption experiments revealed significant signals due to a long-lived transient species with a lifetime of hundreds of nanoseconds for all **TRZ1–3** aggregates in a water dispersion (Fig. S18 and Table S5). The transient absorption spectra recorded *via* laser flash photolysis exhibited negative ground state bleaching around 400 nm and positive ESA above 500 nm, with a spectral shape resembling the triplet absorption as previously determined in solution experiments[17] at least for the **TRZ1** and **TRZ2** aggregates characterized by better signal-to-noise ratios (Fig. S18). The triplet lifetime of the aggregates in a water dispersion was found to be 365 ns for **TRZ1**, 291 ns for **TRZ2**, and 216 ns for **TRZ3** (Table S5). The faster triplet decay observed for the tri-branched system may be possibly linked to a more efficient deactivation channel for the triplet excited state in this case.

Given the significant triplet production observed for **TRZ1–3** in water dispersion and the small ΔE_{ST} values estimated in a previous work,[17] fluorescence kinetics were recorded through TC-SPC also in a long time window of 1–2 μs to look for the possible presence of prompt and delayed emission in DMSO/W mixtures. An in-depth study was performed for the extreme cases of the mono-branched (**TRZ1**) and tri-branched (**TRZ3**) derivatives. When considering mixtures with a large water amount (above 40%), the multiexponential decay fitting of the fluorescence (Table S6) highlighted the presence not only of components with lifetimes of a few nanoseconds (prompt fluorescence) but also of components with lifetimes of hundreds of nanoseconds consistent with the triplet lifetime (delayed fluorescence). The amplitude of such delayed fluorescence was found to be enhanced upon increasing the percentage of water in the mixture (Fig. S19), pointing to an aggregation-enhanced delayed fluorescence behavior. Interestingly, among the aggregates of the three molecules in water dispersion (99%W), the largest amplitude of the delayed fluorescence was revealed in the case of **TRZ3** (Fig. 3A and Fig. S20, Table S6). This result gives a justification to the shorter triplet lifetime measured for **TRZ3** relative to **TRZ1–2**, with **TRZ3** being the compound for which the rISC pathway of triplet decay followed by TADF is relatively more efficient. Time-resolved emission spectra (TRES) were also detected in the microsecond time range by using a micropulsed lamp for the photoexcitation of aggregates of the investigated molecules in water dispersion. A decay of the emission simply resembling the instrumental response function (IRF) was obtained for **TRZ2** and **TRZ3** with TRES consistent with the steady-state emission (Fig. 3B and Fig. S22, S23). On the other hand, for **TRZ1**, also a longer-lived emission of *ca.* 70 μs associated to an emission at *ca.* 640 nm, red-shifted relative to the steady fluorescence, was observed (Fig. 3B and Fig. S21). This peculiar emission may be assigned to the occurrence of room temperature phosphorescence activated in the restricted aggregate environment in the case of **TRZ1**.[22,24,25]

The size of the water-dispersed nanoaggregates was investigated through dynamic light scattering (DLS) measurements. Freshly

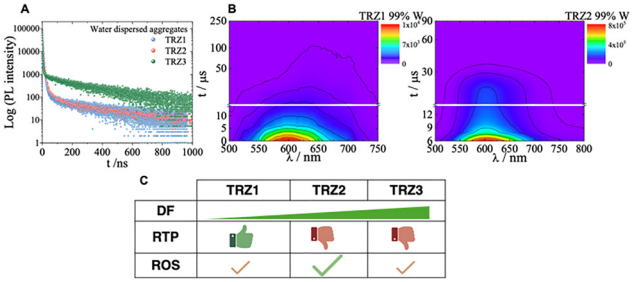

Fig. 3 (A) Fluorescence kinetics obtained *via* TC-SPC for **TRZ1–3** in water dispersion (99%W). (B) TRES matrix in the microsecond time range for **TRZ1–2** aggregates in a water dispersion. (C) Sketch of the DF, RTP, and ROS generation revealed for **TRZ1–3**.

prepared nanoaggregates produced from a DMSO stock solution were generally found to be characterized by two main populations of hydrodynamic diameters of tens and hundreds of nanometers (Fig. S24 and Table S7). A single family of aggregates, peaked at around 140 nm, was instead revealed for **TRZ2**. The size distribution was improved when the preparation was performed by injecting into water a concentrated stock solution in tetrahydrofuran (THF) and when employing sonication, by applying both strategies: a single family of smaller particles was obtained in all cases (Fig. S25–S27 and Table S8). On the other hand, the optical properties of the nanoparticles in water were found to be unaffected by the preparation method (Fig. S10 and S11). The size of the produced organic nanoparticles is compatible with their inclusion within cells.[26] Fluorescence microscopy images were obtained for melanoma (MEL501) and breast cancer (MDA-MB231) cells stained with the DAPI nuclear marker (blue emission) and Phalloidin cellular cytoskeleton marker (green emission). Bright red emission from the **TRZ1–3** nanoparticles was revealed in the perinuclear cellular region (Fig. 4D and Fig. S28 and S29). Dark cytotoxicity was found to be negligible for the investigated compounds, indicating their suitability as bioimaging fluorescent probes (Fig. 4A and Fig. S30). Differently and interestingly, the phototoxicity exhibited by the **TRZ1–3** aggregates against both cancer cell lines after photoexposure was found to be significant, particularly in the case of **TRZ2** (Fig. 4B and Fig. S31). The origin of the observed phototoxicity toward melanoma (MEL501) and breast cancer (MDA-MB231) cells was investigated through experiments aimed at searching for ROS. ROS were found to be generated in the investigated tumor cells well above the control levels upon irradiation when solutions of **TRZ1–3** at 1 or 10 μM concentrations were considered (Fig. 4C and Fig. S32). These results obtained in the cellular environment are in good agreement with fluorimetric tests performed for the **TRZ1–3** aggregates in a water dispersion in the presence of the DCFH2-diacetate ROS probe (Fig. 4C and Fig. S33):[27] the largest ROS production was revealed in the case of **TRZ2**.

In summary, our time-resolved spectroscopic results for purely organic nanoaggregates produced with push–pull phenothiazine–trithienyltriazine derivatives (**TRZ1–3**) in water dispersion highlighted both AIE and significant production of the triplet state, but different deactivation pathways for the latter were tuned by the degree of branching in these molecular structures (Fig. 3C). In particular, an apparent RTP emission was observed for aggregates

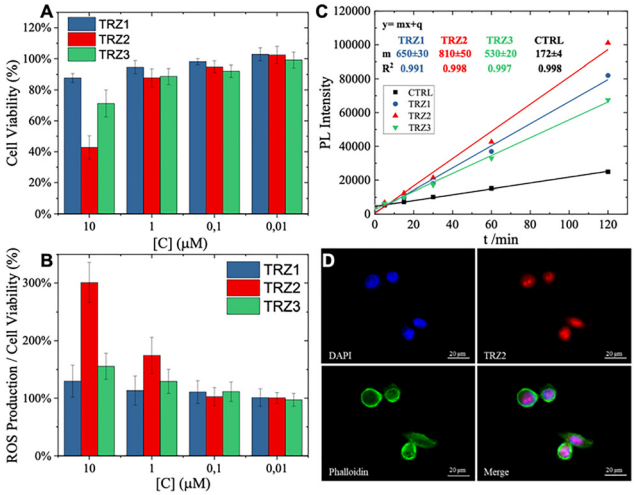

Fig. 4 (A) Phototoxicity of **TRZ1–3** on MEL501 cells with 28 minutes irradiation time (corresponding to 2.59 J cm^{-2}) under UV light. (B) ROS production induced by **TRZ1–3** in MEL501 cells with 28 minutes irradiation time (2.59 J cm^{-2}). Both phototoxicity and ROS production are expressed as the mean of two independent experiments of four replicas each ± SD. 100% corresponds to control mean values. (C) Emission intensity as a function of irradiation time under UV light (3.38 mW cm^{-2}) of water dispersed aggregates of **TRZ1–3** in the presence of DCFH2-dicacetate and for the fluorescent probe alone as a control. (D) Representative fluorescence microscopy images of fixed MEL-501 cells. Cells stained with DAPI (blue, DAPI filter) and 10 μM **TRZ2** (red, TRITC filter) along with relative phalloidin (green, FITC filter) and merged images (image magnification: 60×).

of the dipolar **TRZ1**, while the most important TADF was obtained in the case of the octupolar **TRZ3**. The majority of such orange/red AIE falls into the biological transparency window. On the other hand, the main deactivation channel of the triplet for the quadrupolar **TRZ2** aggregates was found to be the interaction with molecular oxygen, leading to ROS generation and cellular phototoxicity. Organic nanoparticles of these novel dyes therefore hold great potential for applications in imaging-guided PDT.

B. C. acknowledges financial support by the European Union under the Italian Ministry of University and Research (MUR) National Innovation Ecosystem grant ECS00000041 – VITALITY and by the MUR under the PRIN 2022 program (No. 2022RRFJC4). R. M. acknowledges the Science and Engineering Research Board (SERB) No. CRG/2022/000023 and STR/2022/000001, the Council of Scientific and Industrial Research No. 01/3112/23/EMR-II. We are grateful to the DST-FIST grant for the 500 MHz NMR facility and the Sophisticated Instrumentation Centre (SIC), Indian Institute of Technology (IIT) Indore. K. Y. thanks the University Grant Commission (UGC)-New Delhi for the fellowship.

Conflicts of interest

There are no conflicts to declare.

Data availability

The data supporting this article have been included as part of the supplementary information (SI). Supplementary information contains details about the absorption and fluorescence properties, the femtosecond transient absorption results, the nanosecond transient absorption results, the aggregation induced delayed fluorescence, the dynamic light scattering characterization and the biological tests. See DOI: **https://doi.org/10.1039/d5cc05041c**.

Notes and references

1 H. Uoyama, K. Goushi, K. Shizu, H. Nomura and C. Adachi, *Nature*, 2012, **492**, 234–238.
2 M. Y. Wong and E. Zysman-Colman, *Adv. Mater.*, 2017, **29**, 1605444.
3 F. B. Dias, T. J. Penfold and A. P. Monkman, *Methods Appl. Fluoresc.*, 2017, **5**, 012001.
4 C. Montanari, T. Bianconi, M. Sheokand, T. Teunens, G. Cavalletti, J. Cornil, R. Misra and B. Carlotti, *J. Mater. Chem. C*, 2023, **11**, 10893–10904.
5 C. Montanari, N. Ji Tiwari, R. Misra and B. Carlotti, *Chem. – Eur. J.*, 2024, **30**, e202402294.
6 L. Fisher, R. J. Vázquez, M. Howell, A. K. Muthike, M. E. Orr, H. Jiang, B. Dodgen, D. R. Lee, J. Y. Lee, P. Zimmerman and T. Goodson, *Chem. Mater.*, 2022, **34**, 2161–2175.
7 R. J. Vázquez, J. H. Yun, A. K. Muthike, M. Howell, H. Kim, I. K. Madu, T. Kim, P. Zimmerman, J. Y. Lee and T. G. Iii, *J. Am. Chem. Soc.*, 2020, **142**, 8074–8079.
8 F. Fang, L. Zhu, M. Li, Y. Song, M. Sun, D. Zhao and J. Zhang, *Adv. Sci.*, 2021, **8**, 2102970.
9 S. Qi, S. Kim, V.-N. Nguyen, Y. Kim, G. Niu, G. Kim, S.-J. Kim, S. Park and J. Yoon, *ACS Appl. Mater. Interfaces*, 2020, **12**, 51293–51301.
10 C. Si, W. L. Primrose, Y. Xu, Z. M. Hudson and E. Zysman-Colman, *Adv. Opt. Mater.*, 2025, **13**, 2402576.
11 Z. Li, J. Lu and X. Li, *Chem. – Eur. J.*, 2024, **30**, e202401001.
12 Y. Li, M. Tian, R. Wang, X. Lu, K. Ren, Y. Liu and P. Liu, *J. Mater. Chem. B*, 2025, **13**, 10071–10084.
13 F. Terenziani, A. Painelli, C. Katan, M. Charlot and M. Blanchard-Desce, *J. Am. Chem. Soc.*, 2006, **128**, 15742–15755.
14 F. Ricci, B. Carlotti, B. Keller, C. Bonaccorso, C. G. Fortuna, T. Goodson, F. Elisei and A. Spalletti, *J. Phys. Chem. C*, 2017, **121**, 3987–4001.
15 X. Li, L. Huang, G. Baryshnikov, A. Ali, P. Dai, Z. Yang, Y. Sun, C. Dai, Z. Guo, Q. Zhao, F. Zhang and L. Zhu, *Adv. Mater.*, 2025, **37**, 2500236.
16 D. Barman, P. Rajamalli, A. P. Bidkar, T. Sarmah, S. S. Ghosh, E. Zysman-Colman and P. K. Iyer, *Small*, 2025, **21**, 2409533.
17 P. Mancini, C. Montanari, K. Yadav, E. Luzi, R. Misra and B. Carlotti, *J. Mater. Chem. C*, 2025, DOI: **10.1039/D5TC03179F**.
18 X. Cai and B. Liu, *Angew. Chem., Int. Ed.*, 2020, **59**, 9868–9886.
19 B. Liu and B. Z. Tang, *Angew. Chem., Int. Ed.*, 2020, **59**, 9788–9789.
20 A. Cesaretti, T. Bianconi, M. Coccimiglio, N. Montegiove, Y. Rout, P. L. Gentili, R. Misra and B. Carlotti, *J. Phys. Chem. C*, 2022, **126**, 10429–10440.
21 W. Dai, T. Bianconi, E. Ferraguzzi, X. Wu, Y. Lei, J. Shi, B. Tong, B. Carlotti, Z. Cai and Y. Dong, *ACS Mater. Lett.*, 2021, **3**, 1767–1777.
22 T. Bianconi, A. Cesaretti, P. Mancini, N. Montegiove, E. Calzoni, A. Ekbote, R. Misra and B. Carlotti, *J. Phys. Chem. B*, 2023, **127**, 1385–1398.
23 Y. Wang, G. S. He, P. N. Prasad and T. Goodson, *J. Am. Chem. Soc.*, 2005, **127**, 10128–10129.
24 D. Li, Y. Yang, J. Yang, M. Fang, B. Z. Tang and Z. Li, *Nat. Commun.*, 2022, **13**, 347.
25 C. Chen, R. Huang, A. S. Batsanov, P. Pander, Y.-T. Hsu, Z. Chi, F. B. Dias and M. R. Bryce, *Angew. Chem.*, 2018, **130**, 16645–16649.
26 E. Calzoni, A. Cesaretti, A. Polchi, A. Di Michele, B. Tancini and C. Emiliani, *J. Funct. Biomater.*, 2019, **10**, 4.
27 R. Bresolí-Obach, L. Busto-Moner, C. Muller, M. Reina and S. Nonell, *Photochem. Photobiol.*, 2018, **94**, 1143–1150.